

MRI-TRUS fusion for electrode positioning during irreversible electroporation for treatment of prostate cancer

Alexander D. J. Baur
Federico Colletini
Judith Enders
Andreas Maxeiner
Vera Schreiter
Carsten Stephan
Bernhard Gebauer
Bernd Hamm
Thomas Fischer

ABSTRACT

We aimed to introduce an approach for image-guided positioning of electrodes for irreversible electroporation (IRE) in patients with prostate cancer using a magnetic resonance imaging-transrectal ultrasonography (MRI-TRUS) fusion technique. In 10 consecutive patients with biopsy-proven Gleason score $\leq 3+4$ prostate cancer, 19 G electrodes were inserted into the prostate using a transperineal access. Magnetic resonance images of the prostate acquired before IRE were fused with transrectal ultrasound images acquired during IRE. The position of the ultrasound probe was tracked via a sensor and corresponding magnetic resonance images were calculated in real-time. While MRI allowed delineation of the target volume, the position of the electrodes could be visualized on ultrasound images; the distance between individual electrode pairs was measured. Based on these measurements the software installed on the IRE unit was able to calculate the voltage necessary to generate the electric field for ablation. Using contrast-enhanced ultrasound, changes in perfusion within the ablation zone after IRE were documented. This technique allowed positioning of the electrodes around the target volume under image guidance in all patients treated with IRE. The target lesion and a safety margin were covered within the estimated ablation zone. MRI-TRUS guidance for IRE combines the advantages of good visualization of the target lesion on MRI with the ability of ultrasound to acquire imaging in real-time with a mobile device.

Irreversible electroporation (IRE) is a relatively new ablative technique for focal tumor therapy. A pulsed electric field generated around bipolar or between pairs of monopolar electrodes leads to an irreversible permeabilization of cell membranes and consecutive apoptosis dependent on parameters like field strength and duration of application. No relevant amount of thermal energy is released (1–3). A relatively sharp demarcation results between the ablation zone and surrounding vital tissues; shape and size of the ablation zone can be controlled by the positioning of the electrodes used for generation of the electric field (4). Extracellular structures within the ablation zone appear to be preserved as well as structures of the urinary tract (5). Nerve tissue is damaged but the preserved architecture of the endoneurium may enable regeneration (6).

Initial studies evaluating IRE for the treatment of prostate cancer have shown encouraging results (7). Several studies further evaluating the treatment efficacy are currently being undertaken (8, 9). Purpose of this manuscript is to introduce a new technical approach using an MRI-TRUS fusion technique for positioning of electrodes during IRE in patients with prostate cancer.

Technique

Patient cohort

Patients participating in a prospective study, who underwent IRE of the prostate for treatment of prostate cancer between October 2014 and November 2015, were included. Inclusion criteria were presence of unilateral biopsy-proven prostate cancer confined to the prostate with a Gleason score $\leq 3+4$, lesion size on multiparametric MRI ≤ 20 mm, absence

From the Departments of Radiology (A.D.J.B.,
✉ alexander.baur@charite.de, F.C., J.E., V.S.,
B.G., B.H., T.F.) and Urology (A.M., C.S.), Charité
- Universitätsmedizin Berlin, Berlin, Germany;
Berlin Institute for Urologic Research (C.S.), Berlin,
Germany.

Received 7 June 2016; revision requested 29 July
2016; last revision received 18 October 2016;
accepted 5 December 2016.

Published online 15 May 2017.
DOI 10.5152/dir.2017.16276

You may cite this article as: Baur ADJ, Colletini F, Enders J. MRI-TRUS fusion for electrode positioning during irreversible electroporation for treatment of prostate cancer. *Diagn Interv Radiol* 2017; 23:321–325.

of metastatic disease, and serum prostate specific antigen (PSA) levels ≤ 15 ng/mL. Our institutional review board approved the study. All patients gave their informed consent to participate in this study.

Patient preparation

All patients were treated under general anesthesia and full muscle relaxation since the electric field generated during IRE induces significant muscle contractions. Patients were placed on an operating table in lithotomy position. A transurethral urinary catheter was inserted before the procedure.

MRI-TRUS fusion

A high-end ultrasound unit (Aplio 500, Toshiba Medical Systems) was used in combination with a biplane transrectal ultrasound probe (11CL4, Toshiba Medical Systems). For image fusion proprietary Smart Fusion software installed on the ultrasound unit was used. The ultrasound probe was mounted on a frame developed for the implantation of brachytherapy seeds into the prostate (AccuSeed System 700-010, Tayman Medical). Thus, the ultrasound probe was fixated and the exact depth of rectal penetration as well as its rotation could be controlled (Fig. 1). Via a position sensor attached to the ultrasound probe, the position of the probe could be tracked in real-time in a magnetic field (0.1 T, miniBIRD Receiver).

DICOM data of multiparametric MRI of the prostate acquired within three months before IRE without using an endorectal coil were uploaded to the ultrasound unit. The target lesion was identified on multiparametric MRI and marked with a spherical volume-of-interest on T2-weighted imaging (Turbo spin-echo sequence, 3 mm slice thickness, no gap). The ultrasound probe was inserted into

the rectum in a plane strictly orthogonal to the patient's perineum. Ultrasound images of the prostate were acquired at 8–10 MHz in combination with techniques for image optimization (tissue harmonic imaging, spatial and frequency compounding). The height of the operating table was adjusted until an identical distance between the rectum and the prostate on axial T2-weighted imaging and axial ultrasound images resulted, without major deformation of the prostate.

For image registration selected anatomical landmarks that could be identified consistently in each patient (including the urinary bladder neck, the prostatic-semi-

nal vesicle angles, and the surface of the prostate) were initially marked on sagittal ultrasound images as well as on sagittal T2-weighted imaging. Afterwards, the previously selected landmarks were confirmed on axial ultrasound images as well as on axial T2-weighted imaging starting at the base of the prostate and finishing at the apex. Finally, the target lesion was visualized on axial ultrasound images and the surface of the prostate in proximity to the target lesion was marked on axial T2-weighted imaging as well as on axial ultrasound images. The ultrasound unit provided a digital overlay of the volume-of-interest used to mark the

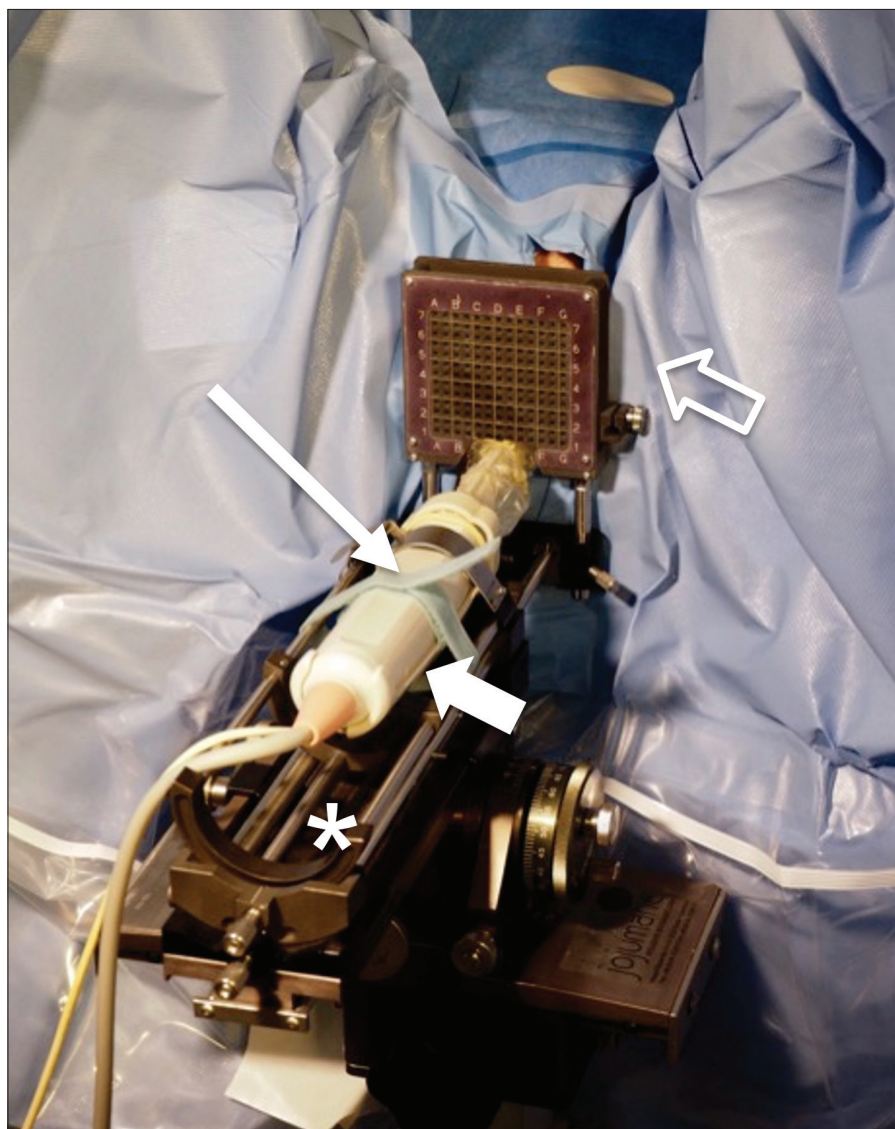


Figure 1. Photograph showing the setting used for treatment of prostate cancer with irreversible electroporation (IRE). A transrectal ultrasound probe (*thin white arrow*) with an attached position sensor (*white arrow*) is mounted on a frame (*asterisk*) that fixates the probe and allows for its exact positioning. A brachytherapy grid (*open white arrow*) is mounted on the frame just caudal of the patient's perineum; the IRE electrodes are inserted through the grid using a transperineal approach. The patient is covered with surgical drapes.

Main points

- MRI-TRUS fusion can be used for image-guided positioning of electrodes for irreversible electroporation (IRE) in patients with prostate cancer.
- This approach combines the advantages of good visualization of the target lesion on MRI with the ability of ultrasonography to acquire imaging in real-time.
- This technique might help to take full advantage of the unique features of IRE allowing to control size, shape, and location of the ablation zone by positioning of the electrodes.

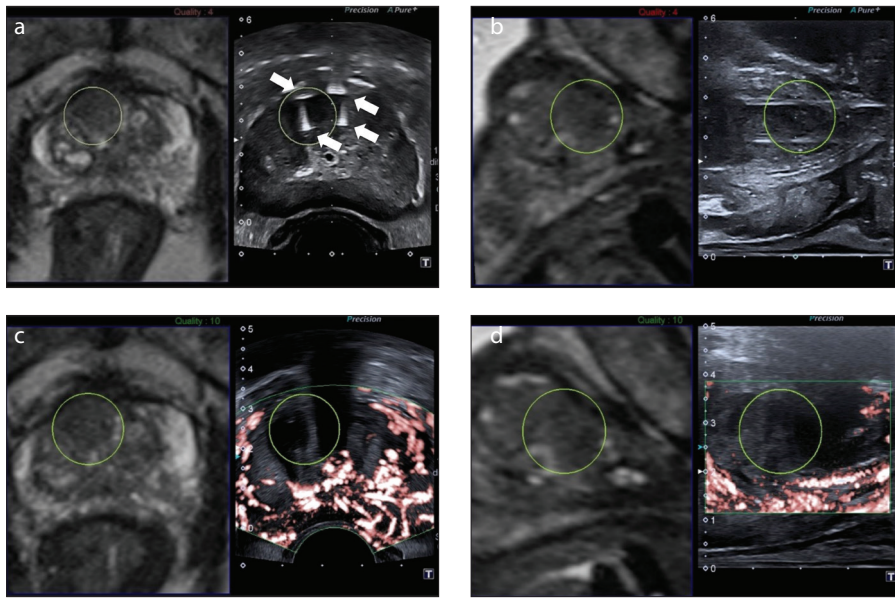


Figure 2. a–d. Example images of magnetic resonance imaging-transrectal ultrasonography (MRI-TRUS) fusion in a 71-year-old patient with Gleason 3+4 prostate cancer in the ventral transition zone. All images show pairs of fused MRI and ultrasound images and represent screenshots from the ultrasound unit. T2-weighted images acquired before IRE are shown on the left (a–d), while fused ultrasound images acquired during IRE are shown on the right (a, b). The target lesion is marked with a spherical volume-of-interest (circle). On axial imaging (a), the position of four electrodes placed peripherally around the target volume can be detected as strong punctiform reflectors (white arrows). Goal is to enclose the target lesion as well as a safety margin between the electrodes. The distance between individual electrode pairs can be measured in this plane. On sagittal imaging (b), the depth of penetration of the electrodes can be detected. Goal is to position the parallel electrodes to cover the target lesion craniocaudally with the tip of the electrode being positioned above the lesion. On axial (c) and sagittal (d) contrast-enhanced ultrasound imaging acquired one day after IRE, a perfusion defect corresponding to the ablation zone can be appreciated. The extension of the perfusion defect matches the estimated ablation zone.

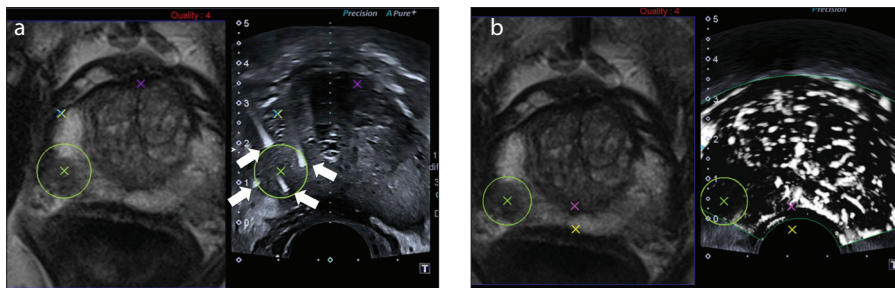


Figure 3. a, b. Example images of MRI-TRUS fusion in a 68-year-old patient with Gleason 3+3 prostate cancer on the right side in the dorsolateral peripheral zone. All images show pairs of fused MRI and ultrasound images and represent screenshots from the ultrasound unit. T2-weighted images acquired before IRE are shown on the left, while fused ultrasound images acquired during IRE are shown on the right. The target lesion is marked with a spherical volume-of-interest (circle). On axial imaging (a) the position of four electrodes placed peripherally around the target volume can be detected as strong punctiform reflectors (white arrows). On contrast-enhanced ultrasound imaging acquired one day after IRE (b) a perfusion defect corresponding to the ablation zone can be appreciated. The extension of the perfusion defect matches the estimated ablation zone.

target lesion on T2-weighted imaging and on ultrasound images. As a result, the location of the target lesion could be tracked on ultrasound images.

A rigid image fusion algorithm was applied. However, deformation of the prostate was minimized due to the fixed position of the ultrasound probe and the fixed position

of the patient on the operating table resulting in a constant angle and distance between the rectum and the prostate during the procedure.

Positioning of IRE electrodes

For generation of the electric field, monopolar needle-like 19 G electrodes (NanoK-

nife, AngioDynamics) were inserted into the prostate through a brachytherapy grid using transperineal access. Goal was to position the electrodes in parallel orientation around the target volume (consisting of the target lesion and a safety margin) covering it within the estimated ablation zone (Figs. 2, 3). The number of electrodes was determined by the shape and size of the target volume. An electric field sufficient for tumor ablation can be generated between each pair of individual electrodes and 5–10 mm around the electrodes. The distance between individual electrodes should be at least 10 mm, not exceeding 20 mm.

The version of the MRI-TRUS fusion system used for positioning of IRE electrodes in the patients described in this manuscript did not offer a digital overlay of the brachytherapy grid on ultrasound images. Therefore, the hole in the grid used for insertion of the first electrode had to be selected based on manual measurements of the distance of the desired position of the electrode and the transrectal ultrasound probe. The hole in the grid used for insertion of additional electrodes was selected based on the location of the first electrode.

Initially, every electrode was advanced deeper into the prostate than the visualized axial image plane showing the target lesion's maximal extension. The position of each electrode was identified on axial ultrasound images after penetrating the visualized image plane as a strong punctiform reflector. The position of the electrodes around the target volume was documented. Now ultrasound images in a sagittal image plane were acquired and corresponding sagittal magnetic resonance images were displayed. The ultrasound probe was rotated to the side of the target lesion and advanced deeper into the rectum until the basal boundaries of the prostate and the seminal vesicles became visible. The tips of the electrodes were identified and the electrodes were pulled back until the tips of all electrodes were located at the same level just above of the target lesion (Fig. 2). The active tip length of the electrodes was adjusted by selective insulation (up to a length of 15 mm) determining the craniocaudal extension of the ablation zone. After switching back to an axial image plane, the ultrasound probe was pulled back until the target lesion was visualized again, as well as the inserted electrodes. The distances between individual electrode pairs were measured.

Generation of the electric field

The distances between electrode pairs were entered manually into the proprietary software installed on the IRE unit (NanoKnife, AngioDynamics). Based on this data the software provided a two-dimensional visualization of the position of the electrodes, as well as the largest diameter of the estimated ablation zone on a single axial image (Fig. 4). For each individual pair of monopolar electrodes the voltage to generate the electric field required for ablation of the target volume was calculated by the software. Ten test pulses were applied and the current graphs of these pulses were reviewed. After review of the current graphs the voltage could be adapted, if necessary. Afterwards, 80 additional pulses were applied. In total, 90 pulses (each with a duration of 70 μ s) were applied. Goal was to achieve a current flow of 20–50 A between each electrode pair.

Documentation of the ablation zone

Every patient underwent transrectal contrast-enhanced ultrasonography (CEUS) the day before and the day after IRE to document changes in perfusion within the ablation zone. The same MRI-TRUS fusion technique that was used for positioning of IRE electrodes was used for CEUS. For CEUS, the novel ultrasound technique of superb microvascular imaging was used in combination with the intravenous application of 2.4 mL of ultrasound contrast agent SonoVue (Bracco). Loss of tissue perfusion in the ablation zone was documented on axial and sagittal ultrasound images (Figs. 2 and 3). The extension of the perfusion defect visualized by CEUS has been shown to correspond well with the extension of the ablation zone on histopathology (10).

Assessment of the agreement between the estimated ablation zone and the actual ablation zone

The area of the estimated ablation zone visualized by the proprietary software installed on the IRE unit was measured using ImageJ analysis software (ImageJ 1.50i, National Institutes of Health). The area of the ablation zone in terms of the largest extension of the perfusion defect visualized by CEUS on a single corresponding axial image was measured using a PACS workstation (Centricity Radiology RA1000, GE Healthcare). Agreement between the

area of the estimated ablation zone and area of the actual ablation zone was assessed by Bland-Altman analysis (IBM SPSS Statistics, Version 21, IBM). In addition, agreement between shape and location of the estimated ablation zone and the actual ablation zone was evaluated visually by an experienced urologist performing a side-by-side reading of multiparametric MRI acquired before IRE, visualization of the position of the electrodes, the estimated ablation zone provided by the proprietary software installed on the IRE unit, and ultrasound images acquired during and one day after IRE.

Results

Ten consecutive patients treated with IRE according to the protocol described above were included in this evaluation. Mean patient age was 62.4 ± 7.3 years. Mean serum PSA before IRE was 9.1 ± 3.6 ng/mL. Gleason score was 3+3 in three patients and 3+4 in seven patients. Mean lesion size was 15 ± 5 mm. Seven lesions were localized in the peripheral zone of

the prostate and 3 lesions were localized in the transition zone. Four electrodes were used in 8 patients and 3 electrodes were used in 2 patients.

In all patients, a satisfactory position of the electrodes was achieved resulting in coverage of the target lesion and a safety margin within the estimated ablation zone. Critical structures including the neurovascular bundle, the urethra, and the rectum could be excluded from the estimated ablation zone to the greatest possible extent. In all patients, a loss of tissue perfusion within the ablation zone was documented by CEUS, while larger capsular vessels stayed intact.

Bland-Altman analysis showed an acceptable agreement between the area of the estimated ablation zone and the actual ablation zone (Fig. 5). Shape and location of the estimated ablation zone and the actual ablation zone showed good agreement on visual evaluation in all patients, resulting in complete coverage of the target lesion within the ablation zone.

No major adverse events were observed during or immediately after IRE.

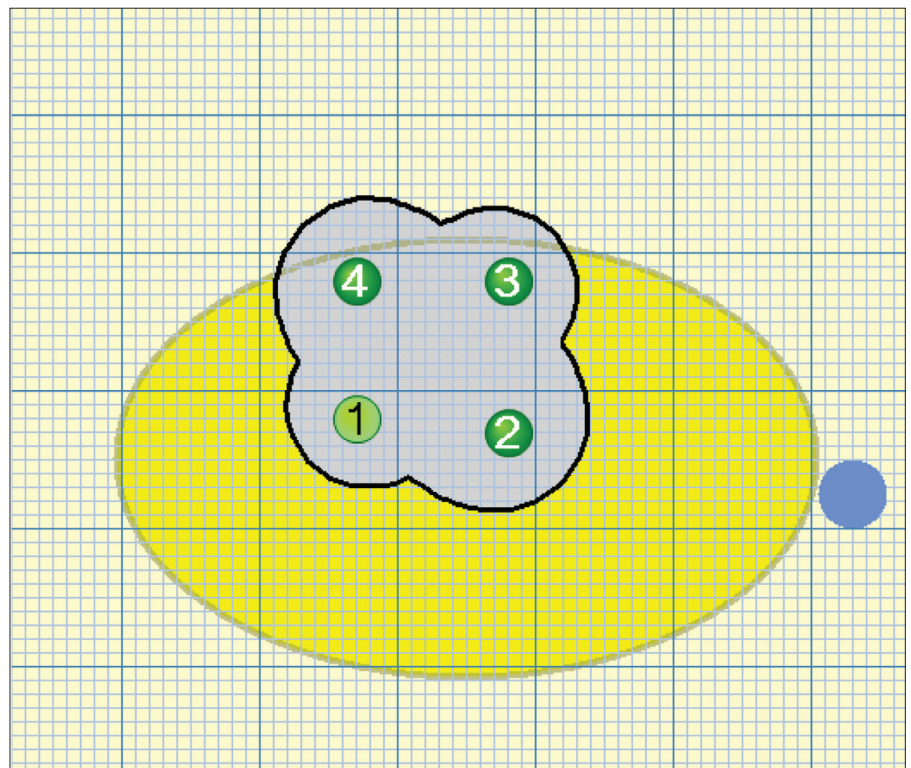


Figure 4. Axial two-dimensional visualization of the position of the inserted electrodes, as well as the resulting estimated ablation zone calculated by the proprietary software installed on the IRE unit. Bold lines represent 10 mm increments and faint lines represent 1 mm increments. Numbered circles represent electrodes ($n=4$). The grey area depicts the estimated ablation zone calculated by the software. The oval yellow area depicts a sketch of the patient's prostate; the depiction of the prostate is not true to scale. The blue circle represents a rotation handle. This example image is taken from the same patient as shown in Fig. 2.

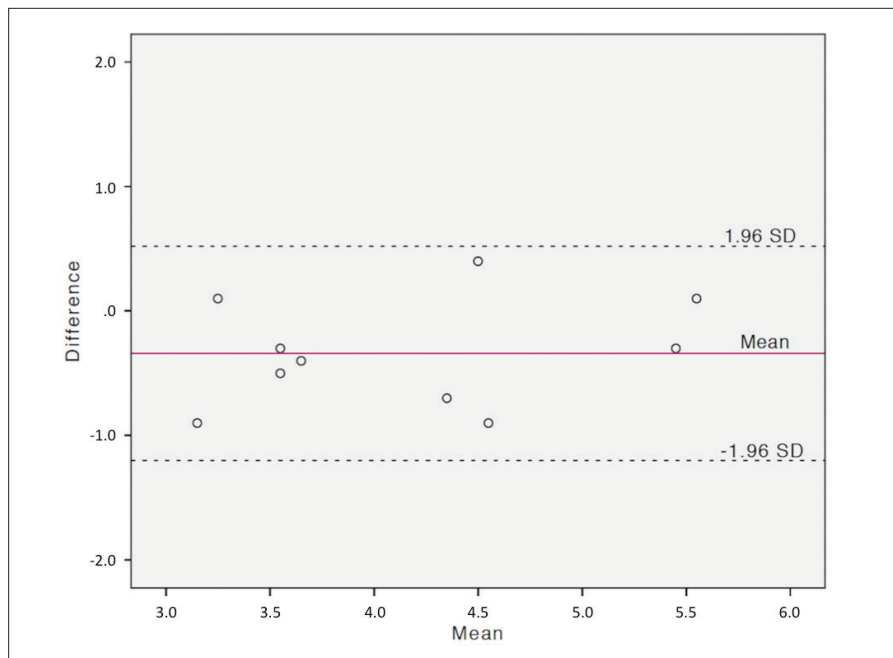


Figure 5. Bland-Altman plot showing the agreement between the area of the ablation zone in terms of the perfusion defect visualized on contrast-enhanced US and the area of the estimated ablation zone visualized by the software installed on the IRE unit. The y-axis represents the difference between the area of the actual ablation zone and the area of the estimated ablation zone in cm². The x-axis shows the mean area of the estimated ablation zone and the perfusion defect in cm². The solid horizontal line represents the mean of all differences; the mean area of the estimated ablation zone was found to be larger than the mean perfusion defect resulting in a mean difference of -0.34 cm². The dashed horizontal lines represent the upper and lower 95% confidence interval limits of the mean difference (0.52 cm² and -1.20 cm²); all individual differences were found to lie within the 95% confidence interval limits.

Discussion

The described MRI-TRUS fusion technique allows positioning of the electrodes under image guidance. Similar fusion techniques have already been established for targeted biopsies of the prostate (11). In a recent feasibility study, MRI-TRUS fusion was used for planning of focal ablative therapy for prostate cancer with high-intensity focused ultrasound (12).

This manuscript offers a description of MRI-TRUS fusion technique for real-time image-guided positioning of electrodes for IRE. Multiparametric MRI can detect clinically significant tumors in the prostate and allows an estimation of tumor volume necessary for planning of the target volume (13). TRUS offers real-time imaging with a mobile device that can be used in the operating room where IRE is performed under general anesthesia. However, prostate cancer often cannot be sufficiently visualized by TRUS alone. Thus, for planning of the target volume ultrasound imaging alone may be insufficient, even if the location of prostate cancer is known from previous multiparametric MRI (14).

MRI-TRUS fusion combines the advantages of multiparametric MRI and TRUS. It has the potential to improve accuracy of IRE for prostate cancer under real-time image guidance.

An important limitation of this study is that no three-dimensional visualization of the estimated ablation zone could be obtained during IRE. In addition, no exact volumetric measurement of the true ablation zone could be performed. Therefore, further work correlating the estimated ablation zone planned based on MRI-TRUS fusion with histopathology is required.

In conclusion, in patients with prostate cancer the described MRI-TRUS fusion technique might help to take full advantage of the unique features of IRE allowing to control size, shape, and location of the ablation zone by positioning of the electrodes. Further studies are necessary to evaluate if this technical approach has a beneficial effect on the clinical outcome.

Conflict of interest disclosure

The authors declared no conflicts of interest.

References

- Davalos RV, Mir IL, Rubinsky B. Tissue ablation with irreversible electroporation. *Ann Biomed Eng* 2005; 33:223–231. [\[CrossRef\]](#)
- Deipolyi AR, Golberg A, Yarmush ML, Arellano RS, Oklu R. Irreversible electroporation: evolution of a laboratory technique in interventional oncology. *Diagn Interv Radiol* 2014; 20:147–154. [\[CrossRef\]](#)
- Savic LJ, Chapiro J, Hamm B, Gebauer B, Colletini F. Irreversible electroporation in interventional oncology: where we stand and where we go. *Rofo* 2016; 188:735–745. [\[CrossRef\]](#)
- Scheffer HJ, Nielsen K, van Tilborg AA, et al. Ablation of colorectal liver metastases by irreversible electroporation: results of the COLD-FIRE-I ablate-and-resect study. *Eur Radiol* 2014; 24:2467–2475. [\[CrossRef\]](#)
- Wendler JJ, Pech M, Porsch M, et al. Urinary tract effects after multifocal nonthermal irreversible electroporation of the kidney: acute and chronic monitoring by magnetic resonance imaging, intravenous urography and urinary cytology. *Cardiovasc Interv Radiol* 2012; 35:921–926. [\[CrossRef\]](#)
- Schoellnast H, Monette S, Ezell PC, et al. The delayed effects of irreversible electroporation ablation on nerves. *Eur Radiol* 2013; 23:375–380. [\[CrossRef\]](#)
- Wendler JJ, Ganzer R, Hadaschik B, et al. Why we should not routinely apply irreversible electroporation as an alternative curative treatment modality for localized prostate cancer at this stage. *World J Urol* 2016; 35:11–20. [\[CrossRef\]](#)
- Valerio M, Dickinson L, Ali A, et al. A prospective development study investigating focal irreversible electroporation in men with localised prostate cancer: Nanoknife Electroporation Ablation Trial (NEAT). *Contemp Clin Trials* 2014; 39:57–65. [\[CrossRef\]](#)
- van den Bos W, de Bruin DM, Muller BG, et al. The safety and efficacy of irreversible electroporation for the ablation of prostate cancer: a multicentre prospective human in vivo pilot study protocol. *BMJ open* 2014; 4:e006382. [\[CrossRef\]](#)
- van den Bos W, de Bruin DM, van Randen A, et al. MRI and contrast-enhanced ultrasound imaging for evaluation of focal irreversible electroporation treatment: results from a phase I-II study in patients undergoing IRE followed by radical prostatectomy. *Eur Radiol* 2015; 26:2252–2260. [\[CrossRef\]](#)
- Cash H, Maxeiner A, Stephan C, et al. The detection of significant prostate cancer is correlated with the Prostate Imaging Reporting and Data System (PI-RADS) in MRI/transrectal ultrasound fusion biopsy. *World J Urol* 2016; 34:525–532. [\[CrossRef\]](#)
- Dickinson L, Hu Y, Ahmed HU, et al. Image-directed, tissue-preserving focal therapy of prostate cancer: a feasibility study of a novel deformable magnetic resonance-ultrasound (MR-US) registration system. *BJU international* 2013; 112:594–601. [\[CrossRef\]](#)
- Turkbey B, Mani H, Aras O, et al. Correlation of magnetic resonance imaging tumor volume with histopathology. *The Journal of urology* 2012; 188:1157–1163. [\[CrossRef\]](#)
- Smeenge M, Barentsz J, Cosgrove D, et al. Role of transrectal ultrasonography (TRUS) in focal therapy of prostate cancer: report from a Consensus Panel. *BJU international* 2012; 110:942–948. [\[CrossRef\]](#)